ANALYSIS OF SHEAR-CRITICAL REINFORCED CONCRETE COLUMNS UNDER VARIABLE AXIAL LOAD

Dimitrios K. Zimos[1], Panagiotis E. Mergos[2], Vassilis K. Papanikolaou[3] and Andreas J. Kappos[4]

Affiliations: [1]PhD, Structural Engineer, Department of Structural Safety, Basler & Hofmann AG, Zurich, Switzerland, ORCID 0000-0002-5937-9161, zimosd@gmail.com; [2]PhD, Senior Lecturer, Civil Engineering Department, City, University of London, London, UK, ORCID 0000-0003-3817-9520; [3]PhD, Assistant Professor, School of Civil Engineering, Aristotle University of Thessaloniki, Thessaloniki, Greece, ORCID 0000-0001-8944-0421; [4]PhD, Professor, Department of Civil Infrastructure and Environmental Engineering, Khalifa University, Abu Dhabi, UAE, ORCID 0000-0002-5566-5021

Photos: [1]  ; [2] 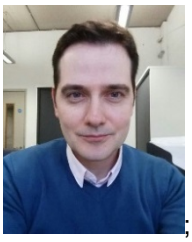 ; [3] 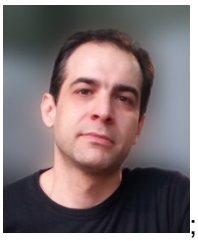 ; [4] 

Text written on: 29/03/2021

Text revised on: 21/09/2021

Number of words in the main text (excluding abstract and references): 4,704

ABSTRACT

Older existing reinforced concrete (R/C) frame structures often contain shear-dominated vertical structural elements, which can experience loss of axial load-bearing capacity after a shear failure, hence initiating progressive collapse. An experimental investigation previously reported by the authors focused on the effect of increasing compressive axial load on the non-linear post-peak lateral response of shear, and flexure-shear, critical R/C columns. These results and findings are used here to verify key assumptions of a finite element model previously proposed by the authors, which is able to capture the full-range response of shear-dominated R/C columns up to the onset of axial failure. Additionally, numerically predicted responses using the proposed model are compared with the experimental ones of the tested column specimens under increasing axial load. Not only global, but also local response quantities are examined, which are difficult to capture in a phenomenological beam-column model. These comparisons

also provide an opportunity for an independent verification of the predictive capabilities of the model, because these specimens were not part of the initial database that was used to develop it.

Keywords: Finite element methods; Failure; Shear

INTRODUCTION

Many existing R/C structures, especially older ones, have been under-designed against seismic loads. Such non-ductile R/C frame structures can undergo vertical progressive collapse, owing to loss of axial load-bearing capacity of their columns, which can be induced by shear or flexure-shear failure followed by further seismic load cycles (Sezen & Moehle 2006). The vertical loads previously carried by a failing member are subsequently redistributed through adjacent horizontal members to neighbouring vertical elements. This leads to a significant increase in the axial load acting on neighbouring columns, altering their non-linear response in terms of strength and deformability (Zimos et al. 2020).

A computationally efficient finite element model was proposed by the authors to model the full-range response of shear- and flexure-shear-critical R/C columns up to the onset of axial failure (Zimos et al. 2018b; Zimos et al. 2018a). The model captures the gradual spread of inelastic flexural and shear deformations as well as shear-flexure-interaction phenomena. Additionally, it can track the response after initiation of shear failure up to the onset of axial failure of R/C columns based on the novel approach of considering the localisation of shear strains in a critical shear length. Following this approach, the proposed formulation provides an objective, physically meaningful and consistent representation of the magnitude and distribution of shear deformations, not only before but also after the onset of shear failure, while avoiding numerical localisation issues related to distributed inelasticity elements.

The authors recently carried out an experimental investigation (Zimos et al. 2020) of the effect of increasing compressive axial load on the non-linear post-peak lateral response of shear and flexure-shear critical R/C columns. Details of the specimens are summarised here, while test results can be found in Zimos et al. (2020). These experiments provide an excellent opportunity to verify key assumptions, upon which the development of the proposed finite element model was based, in particular in the post-peak response domain.

The development of the model was partly based on quantities derived empirically from sizeable databases of experiments on shear-deficient R/C columns with constant applied axial load (Zimos et al. 2018b; Zimos et al. 2018a; Mergos & Kappos 2012). The present paper presents a detailed comparison of the finite element model predictions with the experimentally obtained results. This is the first time the proposed numerical model is applied to shear-dominated R/C columns subjected to increasing axial load. For this purpose, the approach followed to deal with a variable axial load in the post-peak domain is explained in detail. It should also be noted that these specimens were not part of the abovementioned databases, thus providing an opportunity for an independent verification of the model's predictive abilities.

The contribution of this study is not limited to the proposed beam-column model accounting for the effect of axial load increase on the pre-peak and post-peak lateral response of shear-critical R/C columns. The results of this study can also be used to enhance other existing numerical models with the capability to better account for such phenomena, hence modelling the failure of shear-critical column members and by extension the progressive collapse response of R/C buildings more accurately, at a moderate computational cost. Such models are valuable in vulnerability analysis of old buildings for damage states close to collapse.

EXPERIMENTAL CAMPAIGN

To study the effect of axial load increase on the response of shear-dominated columns, shear and flexure-shear critical R/C columns were tested under cyclic lateral load and increasing axial compression (Zimos et al. 2020). Firstly, quasi-static cyclic loading was applied along with constant axial load acting atop the specimen; at a certain point, either just before or just after the onset of shear failure, the vertical load was increased and subsequently the lateral cycling resumed up to the onset of axial collapse. This procedure simulated the response of a column to seismic loading up to a certain point, redistribution of vertical loads due to axial failure of a neighbouring column and continuation of the earthquake action up to axial failure of the column under investigation.

Two sets of three specimens with the same geometry and materials but different reinforcement ratios were tested, one exhibiting a shear-dominated response and one a mixed flexure-shear response. Table 1 presents the design and loading details for each specimen. The specimens

were formed as 715-mm-long cantilevers with a 300×300 (mm) cross-section, thus an aspect-ratio of 2.4. One column per set was tested with constant axial load throughout the response to serve as reference specimen. The focus was on older R/C construction lacking modern design and detailing rules, hence having sparse and poorly anchored transverse reinforcement (90^{o}-hooks and limited anchorage length).

FINITE ELEMENT MODEL

A phenomenological, force-based, spread-inelasticity, beam-column model (Zimos et al. 2018b; Zimos et al. 2018a) has been implemented in the general finite-element program for inelastic dynamic analysis of structures IDARC2D (Reinhorn et al. 2009) with a view to capturing both the pre- and post-peak response of shear deficient R/C members. It is composed of three sub-elements accounting for flexural, shear and anchorage-slip deformations connected in series (Figure 1).

The flexural sub-element (Figure 1c) is divided into an elastic intermediate region and two end regions, where flexural yielding takes place. A spread-inelasticity model is employed to follow the gradual inward penetration of flexural yielding from the ends of the sub-element.

The primary curve, formulated in terms of bending moment vs. curvature at section level, is based on standard flexural analysis with appropriate bilinearisation of the resulting curve. The hysteretic rules employed in the model are presented in detail in Mergos & Kappos (2012).

The anchorage-slip sub-element represents rotations arising at the interfaces of adjacent R/C members due to slippage of reinforcement anchorage in the joints, resulting from bond deterioration. The sub-element (Figure 1e) consists of two concentrated springs at the ends of the element connected by a rigid bar. It has a bilinear primary curve in terms of bending moment vs. end rotations and the hysteretic rules are based on the model proposed by Saatcioglu et al. (1992).

The initial backbone curve of the shear sub-element is formulated in terms of shear force vs. shear distortion at section level, disregarding interaction with flexure. It can be used for elements that have not yielded in flexure as well as for the elastic regions of members that have developed flexural yielding. This curve is defined by the shear cracking point, the onset of yielding of the transverse reinforcement, where maximum shear strength is attained, and a

plateau, where shear strains increase up to the onset of initiation of lateral strength degradation, i.e. the onset of shear failure. Subsequently, a bi-linear descending branch is followed, a shape chosen due to its simplicity, satisfactory correlation with recorded experimental post-peak responses and its versatility in capturing linear, concave and convex types of response (Zimos et al. 2018b). The descending branch is terminated at the point of onset of axial failure, where a column starts losing its axial load-bearing capacity. The definition of the onset of axial failure is both deformation-based and force-based, i.e. either a shear deformation limit is reached or shear strength degrades to zero before this critical deformation is reached.

Prior to the onset of shear failure, the shear sub-element has a flexibility distribution similar to the flexural sub-element (Figure 1d). Shear-flexure interaction is considered in its inelastic end regions, the lengths of which are set equal to the lengths of the respective regions of the flexural sub-element. The initial V-γ curve is modified in these plastic hinge regions, affecting the range between the shear strength corresponding to flexural yielding and the onset of shear failure.

The hysteresis rules adopted in the pre-peak domain of the shear model are based on those by Ozcebe & Saatcioglu (1989) with several improvements for numerical stability in dynamic analysis (Mergos & Kappos 2012; Mergos & Kappos 2008). In the post-peak domain, the hysteresis is largely based on the same rules with various modifications and adaptations, mainly pertaining to post-peak cyclic and in-cycle strength degradation as well as shear strength degradation mirroring (Zimos et al. 2018b).

After the onset of shear failure, the assumption adopted is that flexural and slip-induced deformations do not increase further than their values at peak strength, i.e. the entire post-peak displacement is attributed to shear deformations. These post-peak shear strains after the onset of shear failure are assumed to concentrate in a critical shear length, defined by the diagonal failure planes, which was termed *shear failure localisation* (Zimos et al. 2018b). Inside the critical shear length, the local, post-peak shear hysteretic model is applied. It is noted that this hysteretic model has been calibrated in terms of average post-peak shear strains within the critical shear length (Zimos et al. 2018b). Therefore, the distribution and extent of shear deformations along the member length is predicted in an accurate and objective manner both before and after the initiation of shear failure. Furthermore, by considering the interaction of inelastic flexural and shear deformations at a local level, the proposed approach does not rely

on assumptions regarding the bending moment distribution, hence the actual phenomenon is more realistically captured.

Modelling approach for variable axial load

The finite element model was originally developed based on experiments with constant axial load. However, real-world applications require that variable axial loads and their impact on the lateral response of a column are correctly accounted for. There are, of course, natural axial load fluctuations during an earthquake, especially in the case of corner-columns. However, the most salient aspect of this phenomenon, in the opinion of the authors, pertains to the reduction of axial load in a column occurring after the onset of loss of its axial load-bearing capacity (Nakamura & Yoshimura 2014) and the simultaneous increase of axial load in its neighbouring columns (Zimos et al. 2020); the considerable effect of such axial load variations on the response of shear-dominated columns can be clearly seen in these two experimental campaigns.

These axial load redistributions naturally affect mostly, but not exclusively, the post-peak response domain of a column, since they generally take place at an advanced loading stage. Therefore, the post-peak quantities of the model have been treated as functions of the axial load ratio rather than constant values. At any instance of significant axial load change, the values are re-calculated in order to reflect the new level of axial load. For simplification and numerical robustness, only axial load changes of 5% or more trigger a re-calculation, since smaller changes were not found to affect the post-peak response considerably.

The way this change of post-peak values occurs, in case of an axial load change after the onset of shear failure, is that in effect the re-calculation of the new slope(s) of the post-peak descending branch(es) is based upon the strength at the point where the axial load change occurred (details on post-peak model and corresponding formulae in Zimos et al. 2018b). For the deformation at the onset of axial failure, the newly calculated post-peak deformation is added to the deformation at the onset of shear failure. These re-calculations are indicatively presented in Figure 2 for a case of axial load decrease and a case of axial load increase; for a clearer comparison, they both occur at the same point of an initially identical post-peak descending branch, i.e. at a shear strength level of $V_{max,ax,ch}$. The new descending branch

slopes as well as the new post-peak shear deformations, $\gamma_{t,pp,dec}$ or $\gamma_{t,pp,inc}$ respectively, are calculated based on the new axial load and implemented from that point onwards.

Experimental validation of assumptions for the post-peak range

The numerical modelling of the post-peak domain of the proposed finite element model relies on assumptions requiring robust experimental validation. Nevertheless, there has only been limited validation thus far, mainly due to limited availability of the required level of detail in the recorded response quantities in previous experiments.

The assumption that post-peak displacements are attributed to shear deformations, while flexural and slip-induced deformations do not increase further than their values at peak strength, has also been adopted by other similar models (e.g. Sezen 2008; Elwood 2004) and is supported by experimental observations (e.g. Shirai et al. 1996).

Deformation decomposition of the specimens was carried out and presented in the study by Zimos et al. (2020), clearly showing that it is indeed the case that shear displacements increase considerably in the post-peak range both in absolute and even more so in relative terms, while simultaneously flexural and bond-slip displacements tend to decrease. It should be noted that this marked decrease of the latter starts at the displacement level where the onset of shear failure occurs in some of the specimens and one displacement level thereafter in some other specimens. Nevertheless, the general decreasing trend is considered to be well-founded and the model assumption justified, especially taking into account that the decrease is sometimes extremely high after a certain point in the response, while in the model the decrease takes place more gradually.

The second post-peak assumption was based on experimental observations that deformations after the onset of shear failure tend to concentrate in the critical shear length, defined by the diagonal failure planes, i.e. shear failure localisation (Zimos et al. 2018b). In essence, these concentrated shear deformations mainly represent the relative rigid body displacement between

the discrete upper and lower parts of the column along a shear crack; this can be seen indicatively as well as in an actual experimental test of a shear-deficient R/C column in Figure 3 (column length, L, and critical shear length, L_{cr}).

This assumption is validated here against measurements using Digital Image Correlation at representative test specimens (Zimos 2017). Before the onset of shear failure, the lateral displacement field is continuous along the surface of SC_1 (Figure 4a), while discontinuities start to show at a displacement of 12 mm and even more markedly at 15 mm (Figure 4b). This is due to localisation of the horizontal displacement in the shear cracks, which have a non-negligible crack width of about 1-3 mm at the displacement levels of 12 - 15 mm. Especially from 18 mm onwards, this difference becomes striking, reaching values of 10 mm, and the difference between the top and bottom discrete segments of the column is extremely pronounced (Figure 4c).

The column seems to be effectively split into two parts from the onset of shear failure onwards, divided along the side-to-side shear-crack; in reality it consists of four discrete segments, which however can be lumped into two parts in each loading direction, due to closing of the crack corresponding to the other direction. When applying a load to the top segment, the member is deformed mainly through the crack opening. These displacements mainly represent relative rigid body displacements between the discrete upper and lower segments of the column, separated along said diagonal shear-crack(s). In other words, visualizing the column as a set of components connected in series, the crack-interface component (first appearing in the post-peak regime) requires less energy than the other components to achieve a given displacement, hence being the ‘preferred’ mode of deformation over others, following the ‘weak-link-in-a-chain’ principle.

This is further documented in Figure 5, where the lateral displacement profile at the centroidal axis of specimen SC_2 is provided for top displacement levels between 3 mm and 18 mm. The smooth continuous displacement profiles at the initial stages of the response turn into a set of linear parts and kink points after shear-cracks appear on the specimen. Well into the post-peak domain (it is reminded that shear failure initiated at a displacement of 12 mm) with a clearly formed full-depth diagonal crack, displacement profiles become discontinuous, being broken up by the existence of primarily one wide shear crack; the displacement is quite low below the

crack (similar to the 3 or 6 mm profiles), jumping to a much higher value above them and increasing gradually from that point onwards.

This phenomenon simultaneously influences the longitudinal (vertical) direction, as shown in Figure 6, where vertical displacements of the top cross-section (at the level of application of the lateral load) are shown for various displacement level peaks of specimen SC_2. Vertical displacements initially increase with further lateral displacement owing to the accumulation of steel bar elongation (Zimos et al. 2020); displacements as high as 5 mm are reached at the peaks of the displacement levels of 9 mm and 12 mm. Nonetheless, this pattern changes from the onset of shear failure onwards, as a result of shear failure influencing the axial deformations of the specimen. Vertical displacements of the top section are shown to retract after this point, only slightly at the peak of 12 mm, but much more significantly at the next displacement levels. A full-depth diagonal crack starts forming at the displacement of 12 mm and it has formed and opened considerably at 15 mm. Increased axial shortening is recorded in each test, as soon as this happens; in reality, there is no actual shortening of the column itself, but rather the axial load pushes the upper segment of the column relatively to the lower one, causing these negative vertical displacements. As full-depth diagonal cracks open further, it is easier for the upper segment of the column to move downwards when displaced laterally under the influence of the constant axial load, following the ‘weak-link-in-a-chain’ principle.

FINITE ELEMENT MODEL VERIFICATIONS

The proposed finite element model is verified here against the specimens of the experimental series by Zimos et al. (2020). It is recalled that the comparison of numerical against experimental response of these specimens provides an opportunity for independent verification of the finite element model predictive capabilities, as they were not included in the initial databases, upon which the original model was based (Zimos et al. 2018b).

Response envelopes of reference specimens

The envelope (skeleton curve) of specimens FSC_1 and SC_1 (Table 1) with constant axial load was compared with numerical predictions of the proposed model as well as other models and design codes. The envelopes predicted by the Elwood & Moehle (Elwood & Moehle 2006) model, EC 8-3 (CEN 2005) and *fib* MC 2010 (International Federation for Structural Concrete (*fib*) 2010), and a monotonic response predicted by 3D finite element analysis using the program ATENA (Cervenka et al. 2020) are included. The shear capacity according to each code is also included in dashed line. Both original experimental envelopes and P-δ-free curves are plotted in Figure 7.

The ATENA 3D finite element model was set up using isoparametric solid elements, finely meshed at the column itself as well as the area near the base of the column, using a fracture-plasticity constitutive law for concrete, and more coarsely meshed at the rest of the base using an elastic formulation. The reinforcement was modelled as linear rebar elements embedded in the concrete elements and the boundary conditions were modelled by fully restraining the column base nodes. Loading was initially applied as an axial compressive load on the top surface of the column and subsequently as a monotonically increasing horizontal displacement at the loading level with an adequate number of loading steps up to the appearance of a descending branch in the response (of brittle nature due to the effect of shear), whereupon it was terminated.

Notwithstanding the discrepancy in initial stiffness (Figure 7), the ATENA and Zimos *et al*. models seem to match well the experiments in terms of stiffness at yielding, while the Elwood & Moehle model and the code predictions show a certain underestimation. The ATENA and Zimos *et al*. models also account for stiffness pre- and post-flexural-cracking, while the others do not,

leading to higher discrepancy in the first stages of the response.

The commonly adopted “failure” limit of 20% strength degradation is predicted very well by the Elwood & Moehle and Zimos *et al*. models, roughly at 16 mm of displacement. The codes, on the other hand, predict a brittle shear failure in both cases quite early on, at 5-7.5 mm of lateral displacement. ATENA produces a sudden load drop of more than 20% at 11 mm for the SC-specimen, while the last converged step of the FSC-specimen analysis reaches 20 mm.

The post-peak response domain is only predicted by the Elwood & Moehle and Zimos *et al*. models. This stage of the response, especially when hysteresis is also considered, can typically be predicted only in an empirical way rather than via a mechanics-based approach and its relevant quantities are associated with rather large dispersion. The former model seems to overestimate significantly the strength of the elements as well as predicting much higher lateral displacements at axial failure, i.e. between 36-39 mm. The latter model, however, seems to match the experimental response after the onset of shear failure very well.

Hysteretic response of all specimens

The proposed finite element model was applied to all six specimens of the experimental series (Zimos et al. 2020). The accuracy of analytical predictions is illustrated in Table 2.

The proposed beam-column model seems to be capturing the pre- and post-peak hysteretic response of all specimens well (Figure 8). The stiffness is slightly underestimated at the early stages of the pre-peak domain, while it is mostly well predicted at the stage of yielding. The maximum strength is underestimated in specimens FSC_2, SC_2 and SC_3, because the increased axial load in the pre-peak domain leads to a noticeable increase in lateral load resistance, which is not captured by the numerical model, since only parameters related to the range after the onset of shear failure are axial-load-dependent (see Figure 2). The unloading and reloading stiffnesses of the numerical response represent reasonably well the average stiffnesses observed experimentally, both pre- and post-peak. Comparing the predicted values with the experimental ones (Table 2), the displacement at the onset of shear failure is found to be relatively accurately predicted, with an R_{SFD} ranging from 0.970 to 1.225.

The significant strength degradation observed in the post-peak domain of the FSC-specimens is captured fairly well. In particular, the high strength degradation rate after the onset of shear failure of FSC_3 (Figure 8c) and subsequent sudden loss of a major part of lateral load resistance from 12 mm to 15 mm is captured very well in the negative direction of the predicted hysteretic response, but not so well in the positive direction. The post-peak strength degradation predictions are also satisfactory when it comes to SC-specimens, but with slight underestimation.

Regarding lateral displacement at axial failure, a moderate overestimation is observed in all specimens (Table 2) except for SC_1 and SC_3 (Figure 7d,f). The former did not fail axially during the experiment, but reached an almost negligible lateral strength by the end of cycling. This is captured by the model, which is thus shown not to overestimate the strength degradation, nor underestimate the deformation at the onset of axial failure. In the latter case, no axial failure was experimentally observed even when the specimen reached a displacement of 27 mm, while it was predicted by the model to take place at the last displacement level. Although both post-peak strength degradation and displacement at the onset of axial failure are affected by the axial load increase, the model manages to capture them fairly well, which is a notable accomplishment considering the uncertainties involved at this stage of the response.

Energy dissipation is a key characteristic regarding the seismic response of R/C members. Figure 9 presents how the predictions fare with respect to this particular parameter. The energy dissipation of FSC specimens is found to be quite well predicted, with deviations ranging between 5% and 13% (Table 2). As an example, predicted energy dissipation for FSC_3 (Figure 9a) is shown to be on a par with the experimental one all along the entire test. The energy dissipation of SC specimens is shown to be more significantly overestimated compared to the energy dissipated by the members during the cyclic test (Table 2). Figure 9b demonstrates that the cumulative dissipated energy throughout the experimental test and the analysis of SC_2 are on a par up to the displacement level of 12 mm, deviating after that (similarly with SC_1). This is mainly attributed to thinner loops observed experimentally post-peak that are not captured so accurately in the analysis.

Figure 10 shows the hysteretic response of two representative specimens in terms of shear force vs. shear displacement (i.e. displacement due to shear deformations). Shear

displacements are relatively low at the first stages of the response, increasing drastically upon initiation of shear failure; this is something that the analyses capture well. The shear response of FSC_2 seems to be captured quite well, with certain overestimations of the displacements. The predicted shear hysteretic response of SC_2 is overall very close to the experimental one with moderate deviations. Taking into account the difficulty and complexity of capturing individual deformation components for finite element macro-models as opposed to models based on finer modelling approaches, this level of agreement is considered more than satisfactory for the proposed finite element.

In the case of FSC_1, the predicted critical shear length practically coincides with the measured height of 480 mm using diagonal LVDTs (Zimos 2017), making the predicted and measured average shear strain quantities directly comparable. In order to more rigorously assess how post-peak shear failure localisation is captured, a comparison of the shear deformations in this segment is shown in Figure 11. The shear strains are very well predicted all the way through the test, remaining very low (< 0.01) up to the onset of shear failure in agreement with the experimentally recorded ones, while soaring after that. By the end of cycling, they are predicted to reach almost 0.03, while actually reaching 0.025. As a consequence, approximately 60% of the total displacements are shown to be concentrated in the critical shear length at the end of the test.

Besides higher-level agreement, a more in-depth look into individual cycles can further corroborate the accuracy of the predicted against observed response. Figure 12 shows comparisons of selected individual post-peak hysteretic cycles of FSC_1. Numerically predicted total-displacement cycles are found to agree very well with experimental ones, including pinching, which is low in the first post-peak cycles (Figure 12a), but significantly increases towards the end (Figure 12e). The numerical response in terms of shear displacement cycles is similar on average, but there are certain discrepancies at some points in terms of attained maximum/minimum displacement per cycle. Nonetheless, taking into account the difficulty for a model to capture individual displacement components correctly and since the total energy dissipation per cycle is well captured, the match is considered adequate.

In summary, the proposed finite element model is found to fare very well in comparisons of its predicted response with the experimental one, in part due to capturing the effects of axial load variation on the post-peak response of shear-critical R/C elements adequately.

CONCLUSIONS

The authors recently carried out an experimental investigation, which examined the effect of increasing compressive axial load on the non-linear post-peak lateral response of shear, and flexure-shear, critical R/C columns. These experiments were herein used to verify a computationally efficient finite element model previously proposed by the authors, modelling the full-range response of such columns up to the onset of axial failure. To this end, the beam-column model's capabilities were extended to modelling specimens undergoing axial load variations:

- The model was found to fare very well in terms of global response quantities directly or indirectly affected by the axial load increase, i.e. stiffnesses, dissipated energy, strength degradation, and displacement at onset of shear failure.
- The predicted shear deformation response was also shown to match relatively well both locally at the critical shear length as well as along the entire specimen; achieving such level of agreement with individual experimental displacement components especially in the post-peak range entails great complexity and difficulty, hence being a notable achievement for a finite element macro-model.
- These specimens were not used for the calibration of the model itself, thus providing a completely independent verification of its predictive abilities.
- Last but not least, it was experimentally demonstrated that flexural and slip-induced deformations do not increase beyond their values at the onset of shear failure, i.e. the entire post-peak displacement is practically attributed to shear deformations. Furthermore, the assumption of post-peak shear failure localisation was verified, i.e. that post-peak deformations concentrate in the critical shear length defined by the diagonal failure plane(s).

REFERENCES

Cervenka V, Jendele L and Cervenka J (2020) ATENA Program Documentation, Part 1: Theory. Praha, Czech Republic.

Elwood KJ (2004) Modelling failures in existing reinforced concrete columns. Canadian Journal of Civil Engineering **31(5)**: 846–859, doi.org/10.1139/L04-040

Elwood KJ and Moehle JP (2007) Idealized backbone model for existing reinforced concrete columns and comparisons with FEMA 356 criteria. The Structural Design of Tall and Special Buildings **15(5)**: 553–569, doi.org/10.1002/tal.382

European Committee for Standardization (CEN) (2005) Eurocode 8. Design of structures for earthquake resistance. Part 3: Assessment and retrofitting of buildings. EN 1998-3.

International Federation for Structural Concrete (fib) (2010) Model Code 2010: First Complete Draft, doi.org/10.35789/fib.BULL.0055

Mergos PE and Kappos AJ (2008) A distributed shear and flexural flexibility model with shear–flexure interaction for R/C members subjected to seismic loading. Earthquake Engineering & Structural Dynamics **37(12)**: 1349–1370, doi.org/10.1002/eqe.812

Mergos PE and Kappos AJ (2012) A gradual spread inelasticity model for R/C beam–columns, accounting for flexure, shear and anchorage slip. Engineering Structures **44**: 94–106, doi.org/10.1016/j.engstruct.2012.05.035

Nakamura T and Yoshimura M (2014) Gravity Load Collapse of Reinforced Concrete Columns with Decreased Axial Load. In *2nd European Conference of Earthquake Engineering and Seismology*, Istanbul, Turkey.

Ozcebe G and Saatcioglu M (1989) Hysteretic shear model for reinforced concrete members. Journal of Structural Engineering **115(1)**: 132–148, doi.org/10.1061/(ASCE)0733-9445(1989)115:1(132)

Reinhorn A, Roh H, Sivaselvan M et al. (2009) IDARC2D version 7.0: A program for the inelastic damage analysis of structures. University at Buffalo, State University of New York, Buffalo, New York, Technical Report MCEER-09-0006.

Saatcioglu M, Alsiwat JM and Ozcebe G (1992) Hysteretic behavior of anchorage slip in R/C members. Journal of Structural Engineering **118(9)**: 2439–2458, DOI: 10.1061/(ASCE)0733-9445(1992)118:9(2439)

Sezen H (2008) Shear deformation model for reinforced concrete columns. Structural Engineering and Mechanics **28(1)**: 39–52, doi.org/10.12989/sem.2008.28.1.039

Sezen H and Moehle JP (2006) Seismic tests of concrete columns with light transverse reinforcement. ACI Structural Journal **103(6)**: 842–849, doi.org/10.14359/18236

Shirai N, Lejano BA, Adachi H and Nakanishi M (1996) Flexure and shear behavior of high strength reinforced concrete column subjected to high and fluctuating axial load. In *11th World Conference on Earthquake Engineering*, Acapulco, Mexico, Paper No. 1199.

Zimos DK (2017) Modelling the Post-Peak Response of Existing Reinforced Concrete Frame Structures

Subjected to Seismic Loading. PhD Thesis, City, University of London, London, UK. openaccess.city.ac.uk/18531/

Zimos DK, Mergos PE and Kappos AJ (2018a) Modelling of R/C members accounting for shear failure localisation: Finite element model and verification. Earthquake Engineering & Structural Dynamics **47(7)**: 1631–1650, doi.org/10.1002/eqe.3033

Zimos DK, Mergos PE and Kappos AJ (2018b) Modelling of R/C members accounting for shear failure localisation: Hysteretic shear model. Earthquake Engineering & Structural Dynamics **47(8)**: 1722–1741, doi.org/10.1002/eqe.3037

Zimos DK, Papanikolaou VK, Kappos AJ and Mergos PE (2020) Shear-critical reinforced concrete columns under increasing axial load. ACI Structural Journal **117(5)**: 29-39, doi.org/10.14359/51725886

Table 1: Details of column specimens (Zimos et al. 2020)

Specimen	Failure mode	Axial load (kN)	Point of axial load increase	Concrete Strength (MPa)	Transverse reinforcement	Longitudinal reinforcement
SC_1	Shear	180	-	32.8	Ø8/320	12Ø16
SC_2	Shear	180→270	before 1st cycle of 12 mm	27.2	Ø8/320	12Ø16
SC_3	Shear	180→270	before 1st cycle of 15 mm	24.3	Ø8/320	12Ø16
FSC_1	Flexure-Shear	180	-	26.0	Ø8/270	4Ø16+4Ø14
FSC_2	Flexure-Shear	180→270	before 1st cycle of 12 mm	28.3	Ø8/270	4Ø16+4Ø14
FSC_3	Flexure-Shear	180→270	before 1st cycle of 12 mm	27.7	Ø8/270	4Ø16+4Ø14

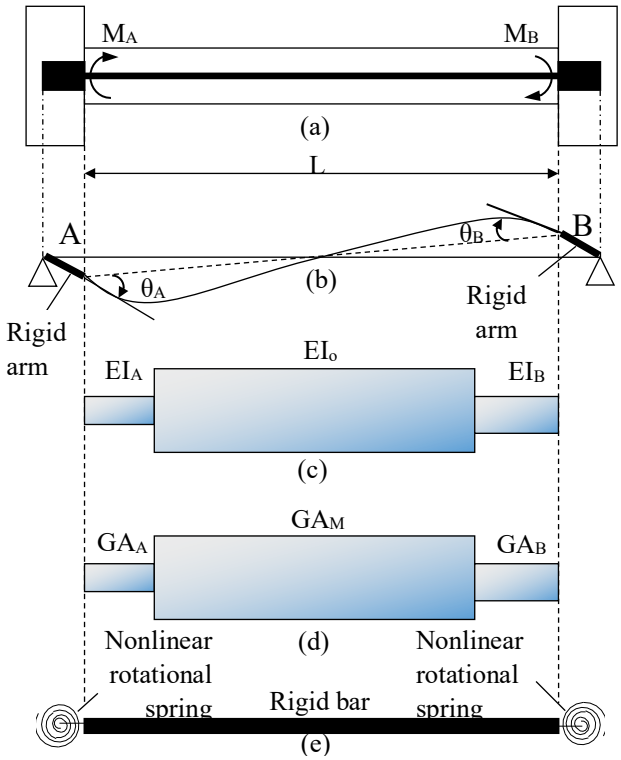

Figure 1: Finite element model: (a) geometry of R/C member; (b) beam–column finite element with rigid offsets; (c) flexural, (d) shear, and (e) anchorage-slip sub-element.

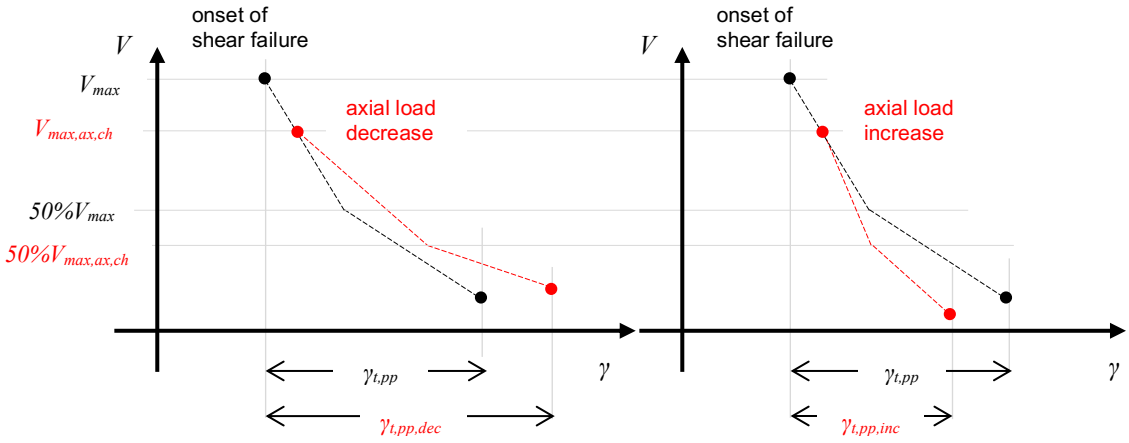

Figure 2: Indicative effect of (left) decreasing or (right) increasing axial load.

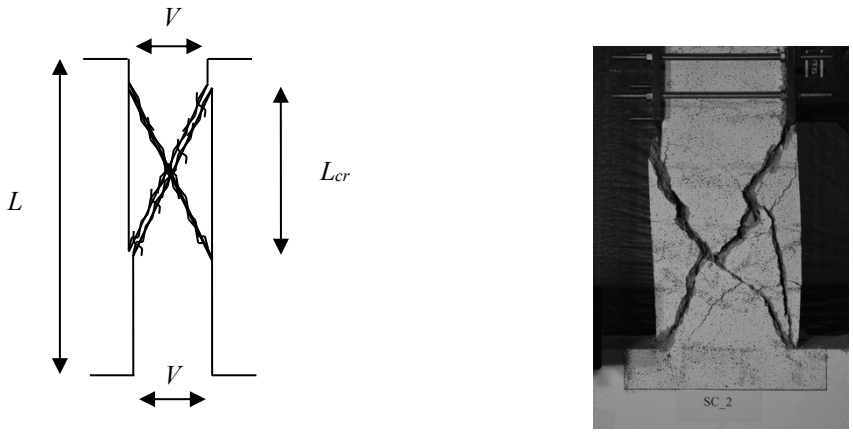

Figure 3: (left) Illustrative sketch of the critical length in a shear-damaged column; (right) Image of axially failed shear-deficient R/C column (Zimos et al. 2020)

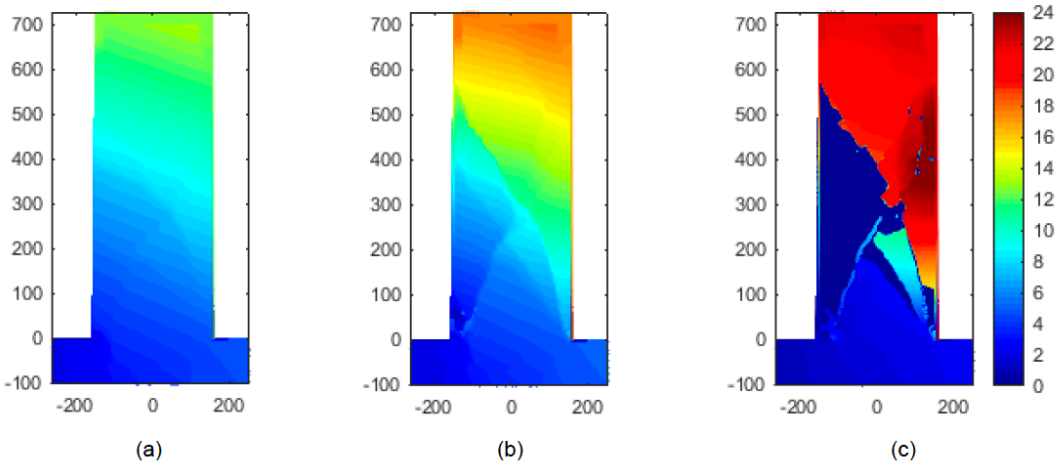

Figure 4: Lateral displacement (mm) contours along the surface of specimen SC_1 for displacement levels of (a) 9 mm, (b) 15 mm, and (c) 21 mm.

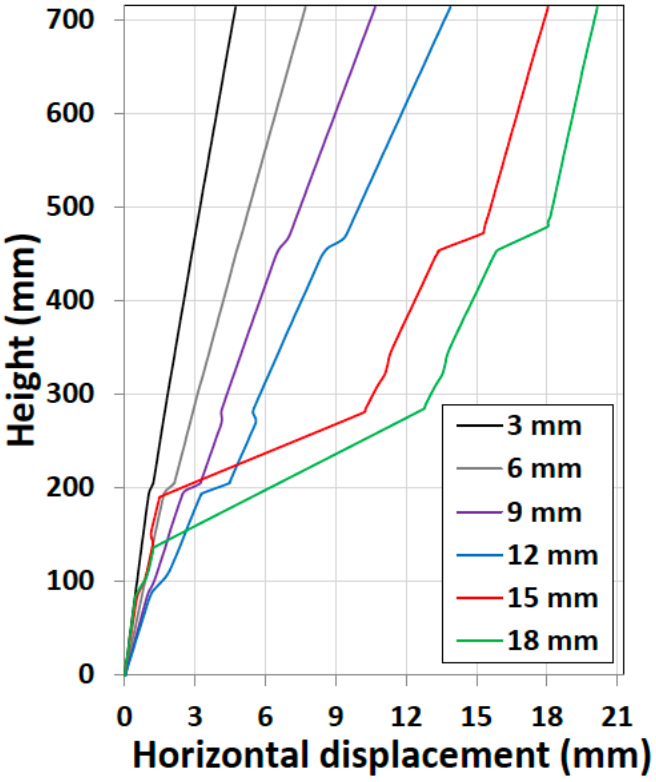

Figure 5: Measured lateral displacement profiles along centroidal axis of SC_2 at displacement level peaks.

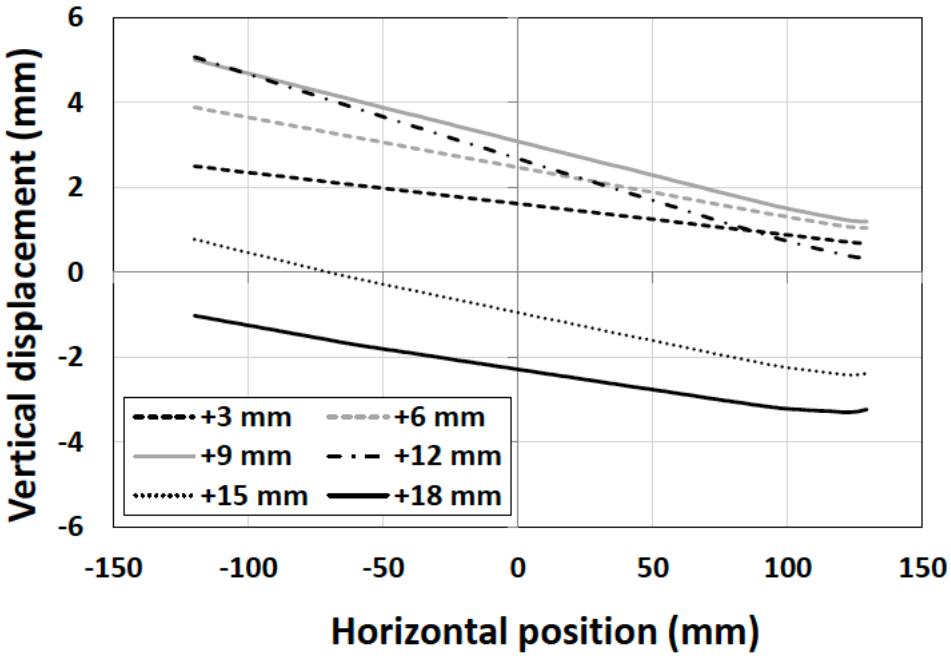

Figure 6: Vertical displacement of top section of SC_2 at various displacement level peaks.

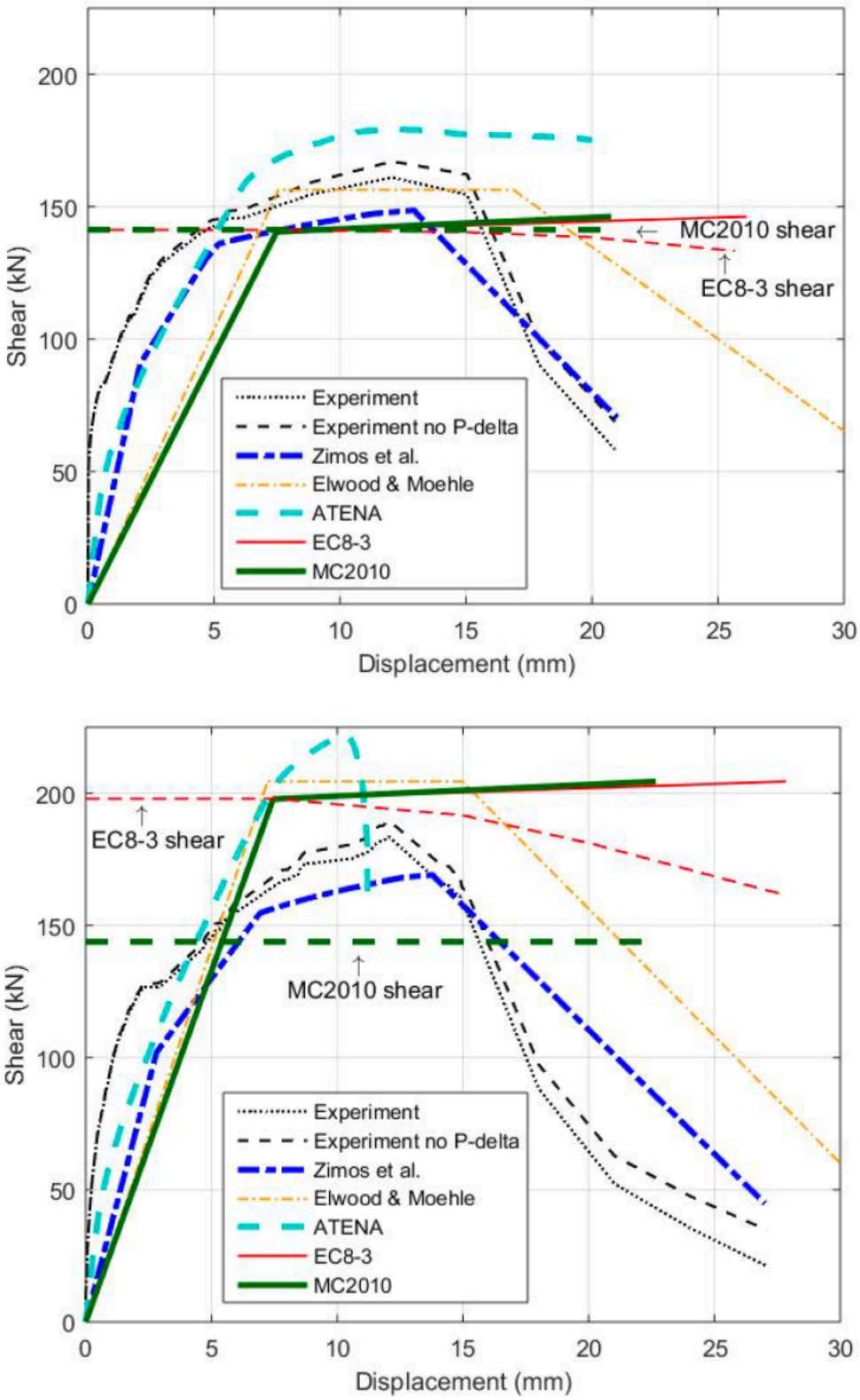

Figure 7: Comparison of experimentally obtained cyclic envelope with the ones predicted by codes and other beam-column models, for (top) FSC_1 and (bottom) SC_1.

Table 2: Ratios of numerically predicted over experimentally measured values of total dissipated energy (R_E), displacement at onset of shear (R_{SFD}) and displacement at axial failure (R_{AFD}) for all specimens.

	R_E	R_{SFD}	R_{AFD}
FSC_1	1.106	0.970	N/A
FSC_2	1.130	0.993	1.173
FSC_3	0.952	0.992	1.472
SC_1	1.174	1.225	N/A
SC_2	1.311	1.075	1.209
SC_3	1.430	0.998	N/A

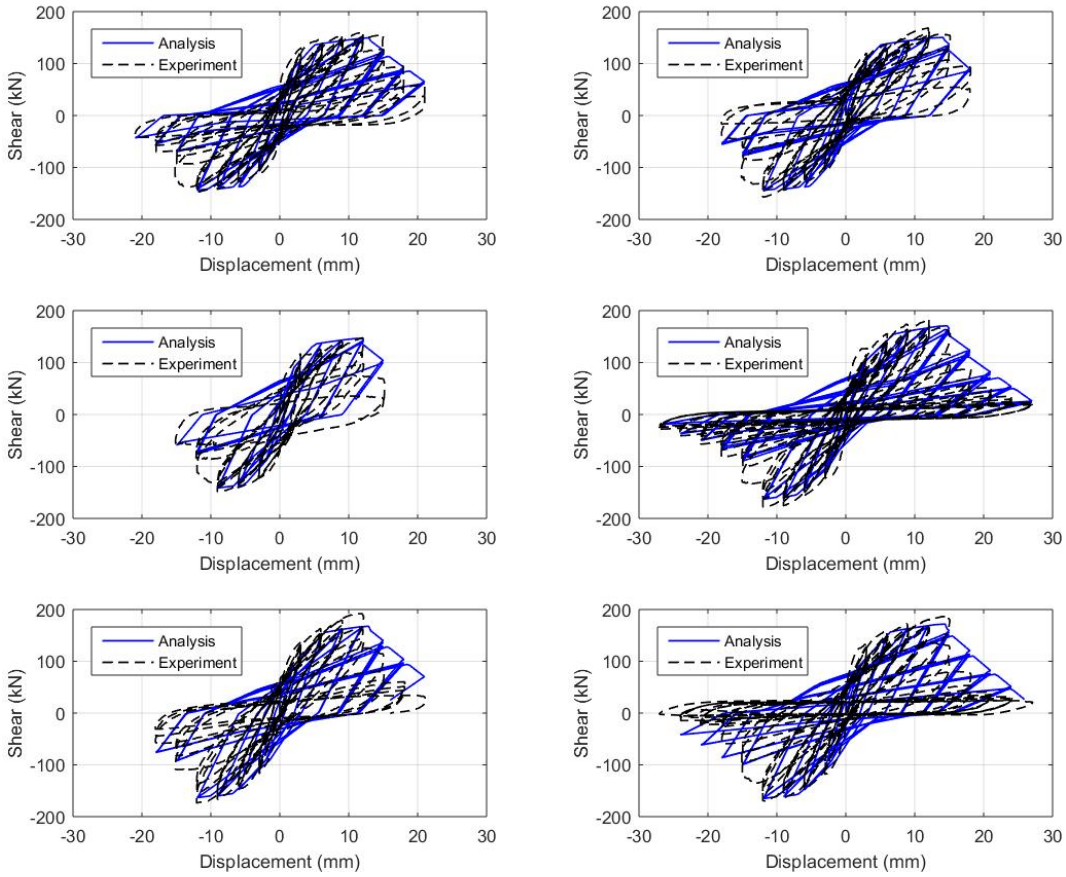

Figure 8: Numerical and experimental hysteretic response of specimens (a) FSC_1, (b) FSC_2, (c) FSC_3, (d) SC_1, (e) SC_2 and (f) SC_3, in terms of shear force against lateral displacement.

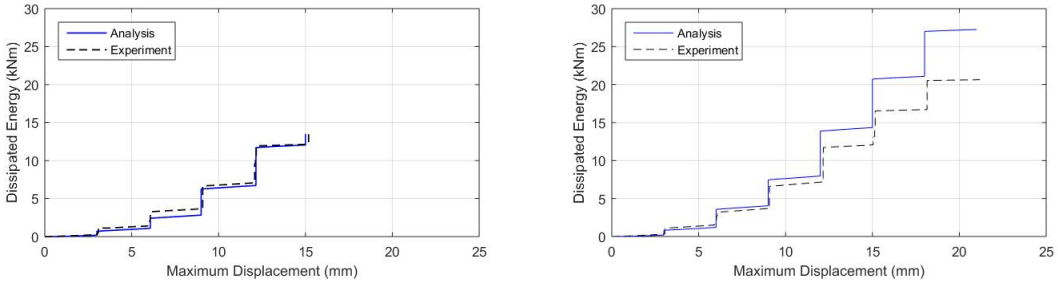

Figure 9: Comparison between predicted and experimental cumulative dissipated energy of specimens (a) FSC_3, and (b) SC_2.

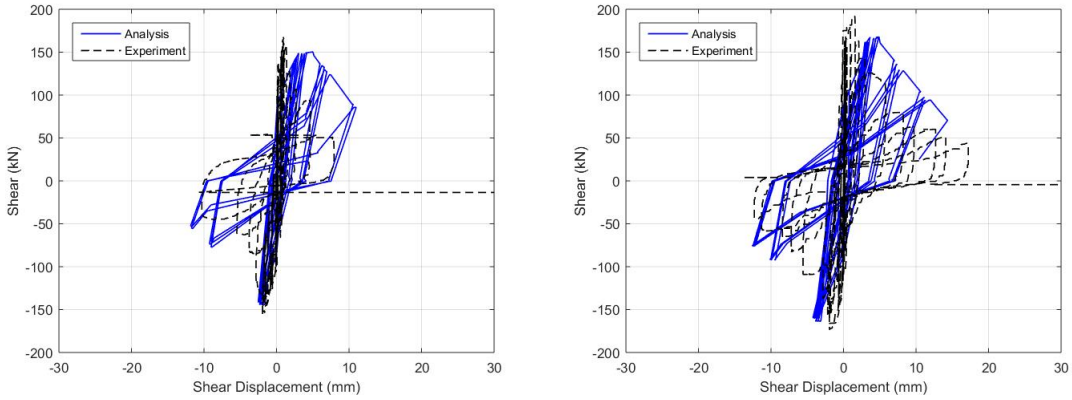

Figure 10: Comparison between numerical and experimental hysteretic response of specimens (left) FSC_2, and (right) SC_2, in terms of shear force against shear displacement.

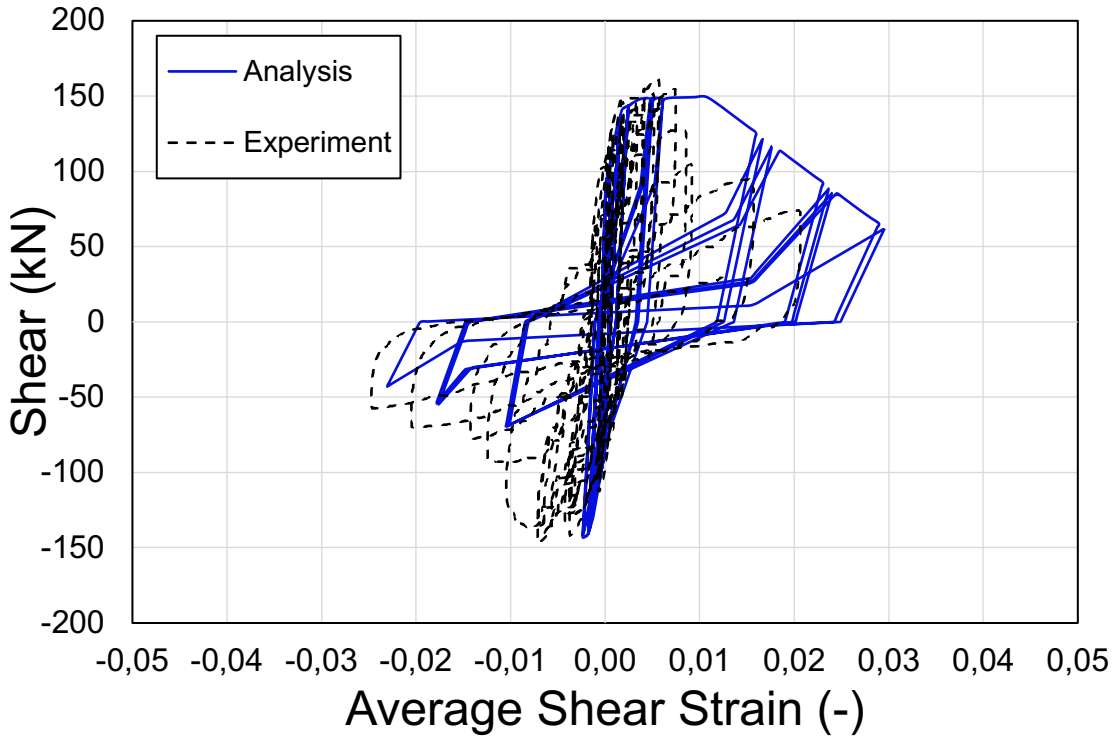

Figure 11: Comparison between predicted and experimental hysteretic response of specimen FSC_1, in terms of shear force against average shear strain in the critical shear length.

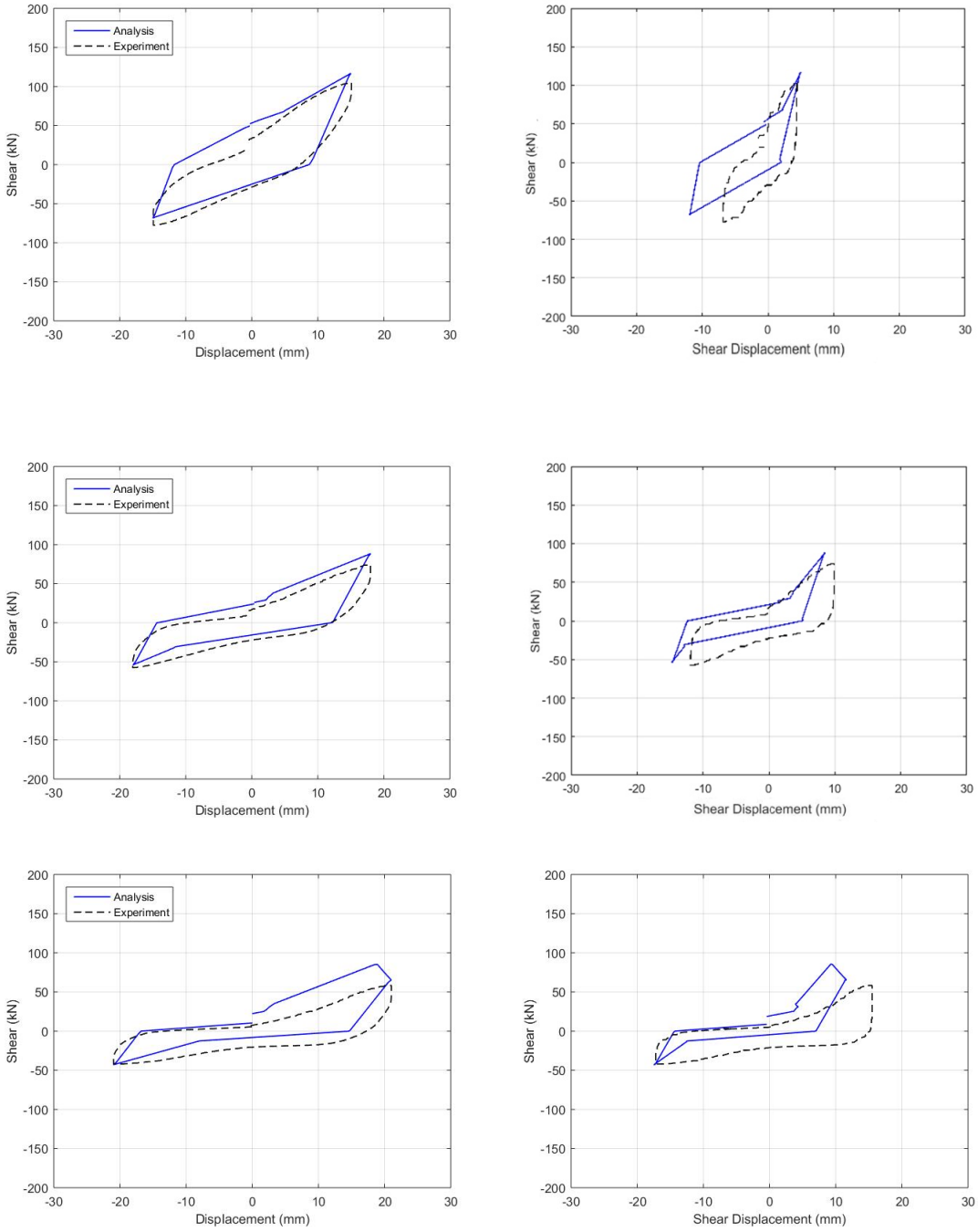

Figure 12: Comparison between individual cycles of numerical and experimental response of FSC_1: (a, b) 3rd cycle at +/-15 mm, (c, d) 2nd cycle at +/-18 mm, and (e, f) 1st cycle at +/-21 mm. (left) Total displacements and (right) shear displacements.